Individual Identification Using Cognitive Electroencephalographic Neurodynamics

Byoung-Kyong Min, *Member, IEEE*, Heung-Il Suk, *Member, IEEE*, Min-Hee Ahn, *Student Member, IEEE*, Min-Ho Lee, and Seong-Whan Lee, *Fellow, IEEE*

***Abstract*— As the brain is a unique biological system that reflects the subtle distinctions in the mental attributes of individual humans, electroencephalographic (EEG) signals have been regarded as one of the most promising and potent biometric signals for discriminating between individuals. However, existing EEG-based user-recognition methods present only a limited range of individual distinctions. In this paper, we propose a novel system of decoding cognitive EEG signals for individual identification with high accuracy. Specifically, we investigate the feasibility of our system, which can recognize an individual based on the discriminative patterns of source-level causal connectivity among brain regions, estimated from scalp-level EEG signals. The EEG signals were produced by a steady-state visual evoked potential-inducing grid-shaped top–down paradigm. This system can, in principle, use top–down cognitive features analyzed by individuals' differently characterized neurodynamic causal connectivities. In this paper, we achieved a maximal accuracy of 98.60% on average in 20 subjects, for whom we estimated causal connectivity in 16 brain regions using 5-s intervals of EEG signals. Our system shows promising initial results toward building a practical identification technology able to recognize individuals by means of brain neurodynamics.**

***Index Terms*— Electroencephalography, causality, cognitive system, identification, support vector machine, top-down processing.**

I. Introduction

TRADITIONAL identification methods that utilize passwords and iris, fingerprint, or face scans [1]–[3] are vulnerable to forged input. Moreover, most provide neither reliable nor efficient identification performance (e.g., a facial recognition system can be spoofed by a photo of a genuine user), and the number of identification systems currently in use is limited. For the purpose of automatic user recognition, there is growing interest in electronic identification using biological signals, such as those from an electroencephalogram (EEG), electromyogram (EMG), or electrocardiogram (ECG). Among these techniques, EEG signals have been regarded as one of the most promising and potent bio-signals for discriminating between individuals [4]–[10]. For instance, identification based on either parametric spectral analysis of EEG signals (with identification accuracy up to 84%) [8] or autoregressive models for single EEG traces (with identification accuracy over 80%) [5] has previously been studied. EEG signals have also been used to decode visual stimuli with high accuracy [11], [12]. Although Palaniappan and Mandic achieved an identity verification rate up to 98.56% using EEG signals [13], there are only a handful of studies that have used EEG-based biometrics. It is worth noting that the brain is considered to be the ultimate target for efficient individual biometric characteristics because it is a unique biological system that reflects subtle distinctions in individual mental attributes.

EEG has been shown to be a versatile and practical tool for neurotechnological applications because of its excellent temporal resolution (approximately 1 ms), portability, and non-invasiveness [14]–[16]. Among EEG-based paradigms, the steady-state visual evoked potential (SSVEP) paradigm provides very accurate and high spectral resolution information (usually less than 0.1 Hz) [17] at high transfer rates [18], [19]. An SSVEP is a physically driven electrical oscillatory response in the brain, induced by the repetitive presentation of a visual stimulus [17]; occipital SSVEPs can be detected at the same flicker frequency (and harmonics) as the flickering stimulus that has been presented. An SSVEP-inducing paradigm has many applications in brain-signal operating systems and neurotechnology [20]–[22].

Given this situation, Min *et al.* [12] recently proposed a new SSVEP-based top-down paradigm, as shown in Fig. 1 and Supplementary Video Clip 1. Using an SSVEP-inducing grid-shaped flickering line array, individually characteristic top-down cognitive features could be extracted from individuals' EEG signals for the purpose of automatic user identification. Unlike bottom-up processing, which is physically driven by external properties, top-down processing efficiently reflects individuals' different and subjective mental neurodynamics. Accordingly, their characteristics are unique for each individual and thus can be used efficiently as a discriminative and exclusive brain fingerprint. Hence, this study proposes a novel individual identification technique using human top-down EEG signals.

II. Materials and Methods

A. Participants and Procedures

Twenty healthy native Korean speakers (10 males and 10 females; age 25.7 (mean) ± 4.6 (s.t.d.) years) partici-

Manuscript received January 12, 2017; revised April 14, 2017; accepted April 27, 2017. Date of publication May 2, 2017; date of current version June 20, 2017. This work was supported by the ITRC program (IITP-2017-2016-0-00464), the IITP grant (B0101-15-0307), and the BSR program (2015R1A1A1A05027233), which are funded by the Ministry of Science, ICT, and Future Planning through the National Research Foundation of Korea. The associate editor coordinating the review of this manuscript and approving it for publication was Prof. Yunhong Wang. *(Corresponding author: Byoung-Kyong Min.)*

The authors are with the Department of Brain and Cognitive Engineering, Korea University, Seoul 02841, South Korea (e-mail: min_bk@korea.ac.kr; hisuk@korea.ac.kr; tigoum@korea.ac.kr; mh_lee@korea.ac.kr; sw.lee@korea.ac.kr).

Color versions of one or more of the figures in this paper are available online at http://ieeexplore.ieee.org.

Digital Object Identifier 10.1109/TIFS.2017.2699944

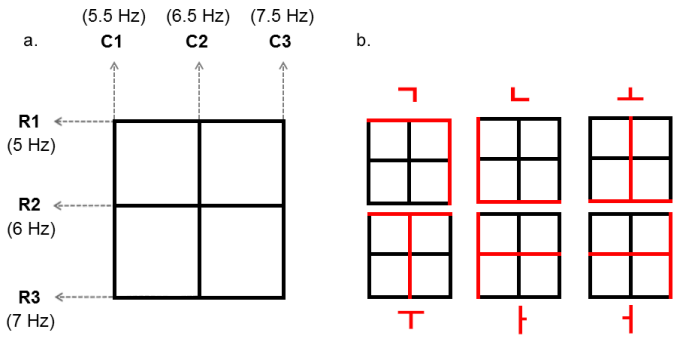

Fig. 1. Schematic of an SSVEP-inducing grid-shaped line array. (a) Grid-shaped line array consisting of 3 rows (R1–R3) and 3 columns (C1–C3) of individually flickering lines. (b) Examples of an attended flickering line composite (in red) when a participant pays particular attention to the Korean letters ㄱ, ㄴ, ㅗ, ㅜ, ㅏ, and ㅓ while looking at the flickering grid-shaped line array [12].

pated in this study. The study was conducted in accordance with the ethical guidelines established by the Institutional Review Board of Korea University and the Declaration of Helsinki (World Medical Association, 2013). Participants had normal or corrected-to-normal vision and provided informed consent prior to the study.

In order to present a mentally generated letter within the participant's restricted visual angle to evoke a corresponding SSVEP, a 6 cm × 6 cm grid-shaped line array was designed (see Fig. 1 and Supplementary Video Clip 1). In this array, 3 rows (R1–R3 in Fig. 1a) and 3 columns (C1–C3 in Fig. 1a) of lines with a mean luminance of 136.26 cd/m^2 were illuminated on a black monitor (Full HD LED 27-in., S27B550, Samsung, Seoul, Korea). Each line had a thickness of 6 mm and the distance between two adjacent rows or columns was 1 cm. This grid-shaped line array was within a visual angle of 6.4° at a distance of 65 cm [23], falling on the retinal region centered at the fovea (the most sensitive portion of the retina) without macroscopic eye movement. In order to generate individual SSVEPs based on each flickering line, each row and column had an individual flickering frequency between 5 and 7.5 Hz (see Fig. 1a); these frequencies have been shown to be effective in inducing SSVEPs in humans [24], [25]. A sampled sinusoidal stimulation method [26] was used to implement visual stimulus presentation on the LED screen for eliciting SSVEP responses.

The underlying concept behind decoding a participant's thoughts using SSVEPs induced by our grid-shaped line array is as follows. When a participant pays attention to a subset of flickering lines, whose combination represents the shape of a letter or symbol, we expect that the frequencies corresponding to those lines are detected as dominant SSVEP features. The frequencies driving the SSVEP signals can be analyzed using a pattern recognition algorithm (detailed in the *Analysis* section) and decoded to determine the participant's identity based on his or her own target signal patterns. The experiment comprises four blocks with a short break in between; each block includes 60 trials. In each block, six predefined Korean letters (ㄱ, ㄴ, ㅗ, ㅜ, ㅏ, and ㅓ) were cued 10 times each for participants to conceive of by a 1-s auditory cue presented 500 ms before the onset of a flickering grid-shaped line array; that is, the participants were instructed to simultaneously attend to two lines that jointly compose a letter. The auditory cues for each letter stimulus were presented in a random order. In order to form ㄱ, R1 and C3 in Fig. 1a should be simultaneously attended. Similarly, R3 and C1 for ㄴ, R3 and C2 for ㅗ, R1 and C2 for ㅜ, R2 and C1 for ㅏ, and R2 and C3 for ㅓ. Inter-trial intervals ranged from 1000 ms to 1500 ms, centered at 1250 ms. After a 1-s auditory cue (an analog instruction sound) pronouncing the Korean letter to which a participant was required to attend, and a subsequent 500 ms buffer period, the grid-shaped line array was presented for 5 s. During this time, the participant was asked to focus his or her attention on the instructed combination of the two corresponding lines among the six flickering lines.

B. EEG Acquisition

EEG signals were measured using a BrainAmp DC amplifier (Brain Products, Germany) with 32 Ag/AgCl electrodes in an actiCAP (Brain Products, Germany) in accordance with the international 10-10 system. An electrode was placed on the tip of the nose as reference, and a ground electrode was placed at electrode AFz. Electrode impedances were maintained below 5 kΩ prior to data acquisition. The EEG was recorded at 500 Hz. Eye movement activity was monitored with an electro-oculogram (EOG) electrode placed sub-orbitally on the left side, and vertical and horizontal electro-ocular activity was computed using two pairs of electrodes placed vertically and horizontally with respect to both eyes (i.e., Fp1 and EOG for the vertical EOG, F7 and F8 for the horizontal EOG). EOG activity was corrected offline using independent component analysis (ICA) [27]. The EEG was segmented from 500 ms pre-stimulus to 5000 ms post-stimulus for each trial. EEG epochs of amplitude greater than $+100$ μV or less than -100 μV and included a gradient greater than 50 μV/ms were automatically excluded. For each EEG epoch, the segment was analyzed in the time window from stimulus onset (i.e., time zero) to 5 s post-stimulus. For the same purpose, time windows of 1–4 s post-stimulus and 2–3 s post-stimulus were taken for 3-s and 1-s EEG epochs, respectively.

C. Granger Causal Analysis

The spatiotemporal distribution of brain activity and network behavior provide significant psychophysiological information and it is important to image functional connectivity to understand brain function [28], [29]. As such, Granger causality [30] analysis was used to find essential neurodynamic networks for the grid-shaped top-down SSVEP paradigm. Granger causality analysis is commonly used to estimate directional causal interactions between electrophysiological signals [29]. In particular, directed transfer function (DTF) is a computational method to measure causality among an arbitrary number of signals [31], [32]. To overcome possible misleading by bivariate measures (e.g., coherence analysis) when applied to multivariate systems [33], DTF has been proposed as a method to extract directional information flow between brain structures [34]. DTF can be regarded as one

type of multivariate Granger causality and can be used to handle multichannel signals derived from the coefficients of a multivariate autoregressive (MVAR) model that fits to the data [30]. The ARfit package [35] was used to compute DTF for the estimation of MVAR models. These computations were conducted using the eConnectome software [29], [36], [37], and the resultant functional connectivity was mapped for the experimental condition. The eConnectome software enabled the estimation of cortical source imaging and subsequent connectivity analysis of cortical source activity.

Computing time can be reduced by decreasing the number of regions of interest (ROIs), which is vital for the real-time application of this technology. In this regard, we analyzed identification accuracy by using causal connectivities as a function of the number of ROIs in Section III-A. Based on the most pronounced cortical activity estimated by the eConnectome software, 4, 8, 12, and 16 ROIs were bilaterally selected among 82 Brodmann areas (BA) to map directional connectivity. That is, the four ROIs were the most activated regions (BA 24L(left)/R(right) and 27L/R) during the task. Along with these 4 ROIs, the 8 ROIs additionally included the next four most activated regions (BA 24L/R, 27L/R, 29L/R, and 32L/R). Similarly, the 12 ROIs (BA 24L/R, 27L/R, 29L/R, 32L/R, 40L/R, and 41L/R) and the 16 ROIs (BA 9L/R, 24L/R, 27L/R, 29L/R, 32L/R, 40L/R, 41L/R, and 42L/R) were sequentially selected to compare their decoding performance as a function of the number of ROIs.

Regarding DTF analysis, and thus the number of features, there are two additional factors that should be considered for a practical use of our system. One is the EEG epoch size; and the other is the number of letter stimuli. We predefined three steps of EEG epoch size (1 s, 3 s, and 5 s), and individual identification accuracy was compared as the EEG epoch size increased from 1 s to 5 s. Similarly, accuracy was also analyzed as the number of letter stimuli increased; 1 (ㄱ) → 2 (ㄱ and ㄴ) → 3 (ㄱ, ㄴ, and ㅗ) → 4 (ㄱ, ㄴ, ㅗ, and ㅜ) → 5 (ㄱ, ㄴ, ㅗ, ㅜ, and ㅏ) → 6 (ㄱ, ㄴ, ㅗ, ㅜ, ㅏ, and ㅓ).

EEG signals in the frequency range from 5 Hz to 14 Hz were used for feature extraction. This frequency range includes the stimulus flickering frequencies along with the sum of the letter-corresponding combination frequencies. Source waveforms at all the selected ROIs were estimated and DTF analysis showed directional information flow across sources. The DTF function yields arbitrary values that represent functional connectivity, which are still subject to statistical assessments of their significance [29]. Because the DTF function has a highly nonlinear relation to the time series data from which it is derived, a non-parametric statistical test method based on surrogate data is used to evaluate the significance of the estimated connectivity measures [38]. In this method, we transformed the original time series to the Fourier space, kept the magnitudes of the Fourier coefficients unchanged, but randomly and independently shuffled the phases of the Fourier coefficients. The surrogate data in the Fourier space were then transformed back to the time domain. This process of phase shuffling preserves the spectral structure of the time series, which is suited for DTF analysis because DTF measures frequency-specific causal interactions. After shuffling, the connectivity estimation was applied to the surrogate data. We repeated the shuffling and connectivity estimation procedures 1000 times for each set of source time series, creating an empirical distribution of the DTF values under the null hypothesis that no causal connectivity exists ($p < 0.05$) [38].

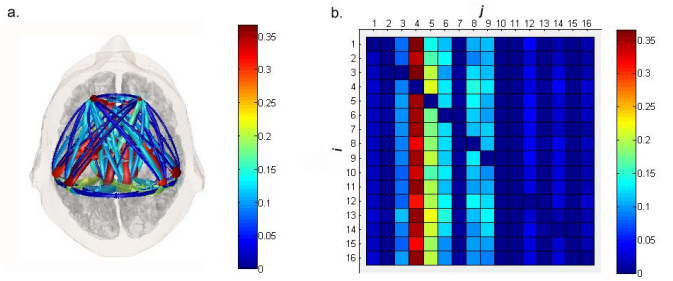

Fig. 2. Grand-averaged topographies of directional cortical activity (a) and the directional flow of brain connectivity (b). Information flow across the 16 × 16 ROIs (j-to-i direction: i, j = 1 for BA 9L, 2 for BA 9R, 3 for BA 24L, 4 for BA 24R, 5 for BA 27L, 6 for BA 27R, 7 for BA 29L, 8 for BA 29R, 9 for BA 32L, 10 for BA 32R, 11 for BA 40L, 12 for BA 40R, 13 for BA 41L, 14 for BA 41R, 15 for BA 42L, and 16 for BA 42R) by Granger causality analysis. Using the estimated time courses of the 16 ROIs, DTF analysis identified directional information flow across cortical sources. Color-scaled directional arrows link two causally connected ROIs when their Granger causality is statistically significant (i.e., $p < 0.05$). Color-scaled arrows in the cortical connectivity image and the pixels in the information flow map represent the degree of causal connectivity (ranging from 0 to 1). The topographical view is from the vertex, with the nasion at the top right of the image.

Finally, for example, we obtained 16 × 16 trial-based information flow maps for the 16 ROIs condition (see Fig. 2) for each subject and extracted individual features from each stimulus category, which were then used for the identification of individuals.

D. Classifier Training and Individual Identification

After DTF analysis, we transformed the information flow matrix into a vector $\mathbf{x}$, which became the input to a classifier that identifies each individual. Specifically, if we consider the number R of ROIs, there are R^2 elements in the DTF matrix. Since we had six different letter stimuli, there were six different DTF matrices. We constructed a feature vector $\mathbf{x}$ by concatenating all the elements of the six DTF matrices. Thus, the dimensions of a feature vector $\mathbf{x}$ are $6 \times R^2$.

For individual identification, we utilized a linear support vector machine (SVM) that performs strongly in many applications [39], [40]. However, since an SVM is basically a binary classifier, it is not directly applicable to our individual identification system (i.e., a multi-class classification task). Typically, there are two different approaches for multi-class classification with a binary classifier: one-against-rest and one-against-one. The one-against-rest method builds K binary classifiers, where K is the total number of classes under consideration, with each binary classifier f_k ($k = 1, \ldots, K$) built between the k^{th} class and K-1 other classes; the one-against-one method builds $K(K\text{-}1)/2$ binary classifiers, with each binary classifier f_{kj} ($k, j = 1, \ldots, K$) built between the k^{th} class and the j^{th} class ($k \neq j$). For reasons of computational efficiency and training costs, we chose to use

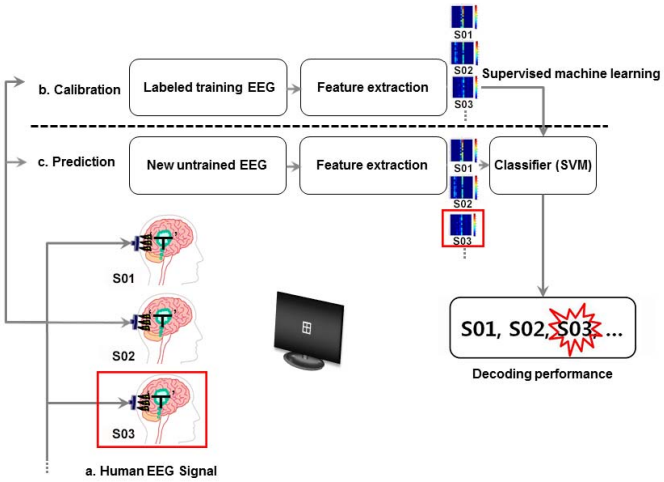

Fig. 3. Overview of the individual identification system using causal brain connectivity patterns. For example, if the causal connectivity pattern of new EEG signals is classified as S03's causal connectivity based on the calibrated data, the system identifies the individual as S03.

the one-against-one approach, which classifies a test sample $\mathbf{x}$ with the following rule:

$$\hat{k} = \underset{k}{\operatorname{argmax}} \sum_{j} f_{kj}(\mathrm{X}) \tag{1}$$

Figure 3 shows the overall configuration of the individual identification system using causal brain connectivity patterns. To validate the effectiveness of the proposed individual identification system, we used a five-fold cross-validation strategy. Specifically, we first randomly partitioned each subject's trials into five subsets such that each subset contained an equal number of samples, i.e., 8 trials per fold. We then used four out of the five subsets for training in a calibration phase and the remaining subset for testing in a prediction phase (Fig. 3), which was thus repeated five times. We recruited 20 participants and obtained 40 trials from each subject for each six-stimulus category. Therefore, with five-fold cross-validation in performance evaluation, we used 640 (20 participants $\times$ 32 trials/subject) and 160 (20 participants $\times$ 8 trials/subject) trials for training and testing, respectively.

To optimize the SVM parameter C, we utilized a nested five-fold cross-validation technique. The labeled training EEG samples from outer cross-validation were further partitioned into five subsets. In an inner cross-validation of the five subsets, four subsets were used for training and the remaining subset was used for validation by changing the value of C, whose space was defined with ten values evenly spaced between 2^{-5} and 2^{4}. After five repetitions (i.e., one validation per subset), we chose the value of C that achieved the maximal average performance and used this value to train the SVM with the outer cross-validation training samples. The LIBSVM toolbox[1] was used for SVM learning and classification. To avoid potential bias that could be incurred during data partitioning, we repeated this process ten times. The performances reported in Section III are the averages across all experiments.

The decoded signals were evaluated to determine whether the individuals' causal brain connectivity patterns, induced by the set of attended flickering lines, could be successfully differentiated; i.e., whether the users of this system were correctly identified. The rates of successful identification of the test data were compared across the different numbers of ROIs, EEG epoch sizes, and numbers of letter stimuli in order to evaluate the decoding performance. In order to statistically examine whether decoding accuracies were significantly different across the experimental conditions, two-tailed paired-sample t-tests were performed. A false discovery rate (FDR) of $q = 0.01$ was used to correct for multiple comparisons, which is known to be commonly acceptable for this purpose [41]. All analyses were performed using MATLAB (ver. R2015b, MathWorks, USA) or SPSS Statistics (ver. 22, IBM, USA).

[1] Available at http://www.csie.ntu.edu.tw/cjlin/libsvm/.

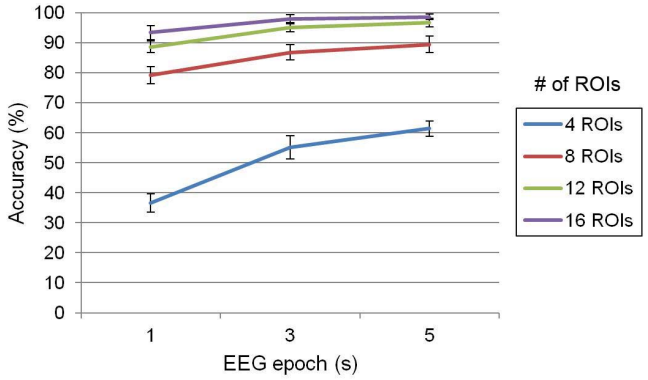

Fig. 4. Identification performance changes as a function of the number of ROIs and EEG epoch size when all six letter stimuli were analyzed. Error bars represent standard deviations.

III. Results

A. Number of ROIs and Identification Performance

We achieved a maximal accuracy of 98.60 $\pm$ 1.00% with the 16-ROI, 5-s EEG epoch, 6-letter stimulus condition, an improvement of 1.89% over the 12-ROI condition. As plotted in Fig. 4, individual identification decoding accuracies ranged from 61.30% (4 ROIs) to 98.60% (16 ROIs) in the 5-s EEG epoch, 6-letter stimulus case. Accuracy gradually increased along with the number of ROIs and EEG epoch size. As shown in Table I, decoding accuracy when using 12 ROIs was not significantly different from that when using 16 ROIs across all the EEG epoch sizes: 1-s EEG epoch (12 ROIs, 88.65%; 16 ROIs, 93.30%; $t_{19} = -2.53$, non-significant [*n.s.*], FDR corrected), 3-s EEG epoch (12 ROIs, 95.10%; 16 ROIs, 97.85%; $t_{19} = -3.18$, *n.s.*, FDR corrected) and 5-s EEG epoch (12 ROIs, 96.65%; 16 ROIs, 98.60%; $t_{19} = -2.10$, *n.s.*, FDR corrected).

B. EEG Epoch Size and Identification Performance

Figure 5 demonstrates that decoding accuracies ranged from 93.30% (1-s EEG epoch) to 98.60% (5-s EEG epoch) when all six letter stimuli and 16 ROIs were taken into account. Accuracy gradually improved as the number of ROIs and EEG epoch size increased. It is noteworthy that decoding accuracies by 3-s EEG epochs were not significantly different from those by 5-s EEG epochs across all ROI conditions (see

TABLE I

STATISTICAL COMPARISONS OF IDENTIFICATION ACCURACY ACROSS DIFFERENT NUMBERS OF ROIS (4, 8, 12, AND 16) IN DIFFERENT EEG EPOCH SIZES (1, 3, AND 5 s) AVERAGED OVER ALL SIX LETTER STIMULI. MULTIPLE COMPARISONS WERE CORRECTED BY FALSE DISCOVERY RATE (FDR)

# of ROIs	1-s epoch	3-s epoch	5-s epoch
4 vs. 8	t_{19} = -12.61, $p < 0.001$	t_{19} = -9.25, $p < 0.001$	t_{19} = -10.36, $p < 0.001$
4 vs. 12	t_{19} = -13.95, $p < 0.001$	t_{19} = -9.91, $p < 0.001$	t_{19} = -9.79, $p < 0.001$
4 vs. 16	t_{19} = -14.47, $p < 0.001$	t_{19} = -10.14, $p < 0.001$	t_{19} = -9.47, $p < 0.001$
8 vs. 12	t_{19} = -4.98, $p < 0.001$	t_{19} = -4.41, $p < 0.001$	t_{19} = -5.40, $p < 0.001$
8 vs. 16	t_{19} = -6.30, $p < 0.001$	t_{19} = -5.29, $p < 0.001$	t_{19} = -4.63, $p < 0.001$
12 vs. 16	t_{19} = -2.53, *n.s.*	t_{19} = -3.18, *n.s.*	t_{19} = -2.10, *n.s.*

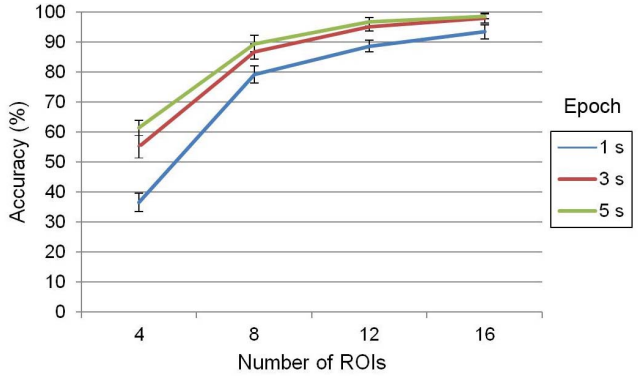

Fig. 5. Identification performance changes as a function of EEG epoch size and the number of ROIs when all six letter stimuli were analyzed. Error bars represent standard deviations.

TABLE II

STATISTICAL COMPARISONS OF IDENTIFICATION ACCURACY ACROSS DIFFERENT EEG EPOCH SIZES (1, 3, AND 5 s) IN DIFFERENT NUMBERS OF ROIS AVERAGED OVER ALL SIX LETTER STIMULI. MULTIPLE COMPARISONS WERE CORRECTED BY FALSE DISCOVERY RATE (FDR)

Epoch size	4 ROIs	8 ROIs	12 ROIs	16 ROIs
1 vs. 3	t_{19} = -5.50, $p < 0.001$	t_{19} = -4.45, $p < 0.001$	t_{19} = -5.30, $p < 0.001$	t_{19} = -4.27, $p < 0.001$
1 vs. 5	t_{19} = -6.26, $p < 0.001$	t_{19} = -5.65, $p < 0.001$	t_{19} = -6.03, $p < 0.001$	t_{19} = -4.74, $p < 0.001$
3 vs. 5	t_{19} = -2.47 *n.s.*	t_{19} = -2.08, *n.s.*	t_{19} = -2.06, *n.s.*	t_{19} = -1.58, *n.s.*

Table II): 4 ROIs (3-s epoch, 55.05%; 5-s epoch, 61.30%; $t_{19} = -2.47$, *n.s.*, FDR corrected), 8 ROIs (3-s epoch, 86.75%; 5-s epoch, 89.45%; $t_{19} = -2.08$, *n.s.*, FDR corrected), 12 ROIs (3-s epoch, 95.10%; 5-s epoch, 96.65%; $t_{19} = -2.06$, *n.s.*, FDR corrected), and 16 ROIs (3-s epoch, 97.85%; 5-s epoch, 98.60%; $t_{19} = -1.58$, *n.s.*, FDR corrected). As shown in Fig. 5, accuracy tends to saturate with more than 12 ROIs; that is, small improvements occur with 16 ROIs compared to 12 ROIs.

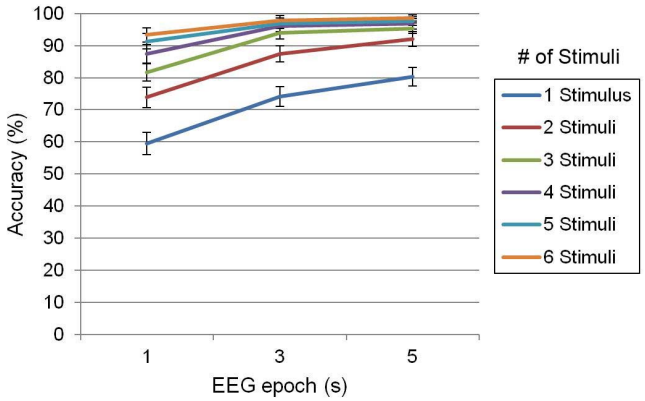

Fig. 6. Identification performance changes as a function of the number of stimuli and EEG epoch size when 16 ROIs were analyzed. Error bars represent standard deviations.

C. Number of Stimuli and Identification Performance

Decoding accuracy ranged from 80.20% (with a single stimulus) to 98.60% (with all six stimuli) in the 5-s EEG epoch, 16-ROI case. Accuracy gradually increased with the number of letter stimuli and EEG epoch size (Fig. 6). It is noteworthy that even with three letter stimuli (ㄱ, ㄴ, and ㅗ), considerable decoding accuracy (95.30%) was achieved, which was not significantly different from the accuracy (97.65%) of the case using five letter stimuli ($t_{19} = -3.03$, *n.s.*, FDR corrected) in the 5-s EEG epoch, 16-ROI condition (see Table III). This small number of letter stimuli reduces classification time.

D. Practicability Optimization

Although further detailed information by more experimental parameters leads to higher system accuracy, this is not economically optimal for a practical system. As shown in Tables 1 and 2, accuracies obtained using 12 ROIs and 3-s EEG epochs are statistically comparable to those obtained using 16 ROIs and 5-s EEG epochs, respectively. Based on these observations, we optimized our system by setting the number of ROIs and EEG epoch size to 12 ROIs and 3 s, respectively.

In addition, taking all six letter stimuli into account for individual identification inevitably increases the number of features and the computing time required for DTF analysis. In this regard, it may be reasonable to sacrifice a small improvement in identification accuracy in order to make our system more practical over a given time domain, as previously mentioned.

In order to empirically estimate overall processing time, the processing times for DTF computation and individual classification by SVM were measured in the 12-ROI case, as shown in Fig. 7. Computing times were positively proportional to the number of letter stimuli and EEG epoch size.

TABLE III

STATISTICAL COMPARISONS OF IDENTIFICATION ACCURACY ACROSS THE DIFFERENT NUMBERS OF LETTER STIMULI IN DIFFERENT EEG EPOCH SIZES AVERAGED OVER 16 ROIS. MULTIPLE COMPARISONS WERE CORRECTED BY FALSE DISCOVERY RATE (FDR)

# of stimuli	1-s epoch	3-s epoch	5-s epoch
1 vs. 2	t_{19} = -8.18, $p < 0.001$	t_{19} = -12.21, $p < 0.001$	t_{19} = -5.95, $p < 0.001$
1 vs. 3	t_{19} = -10.13, $p < 0.001$	t_{19} = -10.53, $p < 0.001$	t_{19} = -6.38, $p < 0.001$
1 vs. 4	t_{19} = -12.92, $p < 0.001$	t_{19} = -11.78, $p < 0.001$	t_{19} = -6.36, $p < 0.001$
1 vs. 5	t_{19} = -13.75, $p < 0.001$	t_{19} = -11.68, $p < 0.001$	t_{19} = -6.88, $p < 0.001$
1 vs. 6	t_{19} = -14.75, $p < 0.001$	t_{19} = -11.70, $p < 0.001$	t_{19} = -6.76, $p < 0.001$
2 vs. 3	t_{19} = -7.67, $p < 0.001$	t_{19} = -5.20, $p < 0.001$	t_{19} = -4.06, $p < 0.005$
2 vs. 4	t_{19} = -9.94, $p < 0.001$	t_{19} = -6.86, $p < 0.001$	t_{19} = -4.82, $p < 0.001$
2 vs. 5	t_{19} = -10.37, $p < 0.001$	t_{19} = -7.11, $p < 0.001$	t_{19} = -5.36, $p < 0.001$
2 vs. 6	t_{19} = -11.70, $p < 0.001$	t_{19} = -7.57, $p < 0.001$	t_{19} = -5.29, $p < 0.001$
3 vs. 4	t_{19} = -6.43, $p < 0.001$	t_{19} = -5.23, $p < 0.001$	t_{19} = -1.89, *n.s.*
3 vs. 5	t_{19} = -6.94, $p < 0.001$	t_{19} = -4.81, $p < 0.001$	t_{19} = -3.03, *n.s.*
3 vs. 6	t_{19} = -8.04, $p < 0.001$	t_{19} = -5.71, $p < 0.001$	t_{19} = -3.71, $p < 0.005$
4 vs. 5	t_{19} = -4.98, $p < 0.001$	t_{19} = -1.80, *n.s.*	t_{19} = -2.54, *n.s.*
4 vs. 6	t_{19} = -6.14, $p < 0.001$	t_{19} = -3.18, $p < 0.01$	t_{19} = -3.35, $p < 0.005$
5 vs. 6	t_{19} = -3.86, $p < 0.005$	t_{19} = -3.80, $p < 0.005$	t_{19} = -2.35, *n.s.*

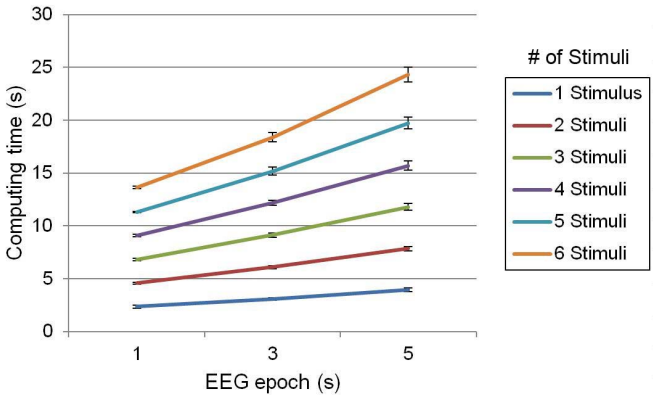

Fig. 7. Change in computing time of individual identification as a function of the number of letter stimuli and EEG epoch size when using 12 ROIs. Error bars represent standard deviations.

Table IV demonstrates the trade-off between identification accuracy and computing time as a function of the number of letter stimuli under the 12-ROI, 3-s EEG epoch condition. For instance, three letter stimuli yielded relatively good performance, with an accuracy of 86.39% and a reasonable computing time of 9.13 s on average. Consistently, Section III-C shows that only the three-letter stimulus set produced statistically comparable accuracy to the five-letter stimulus set. To this end, we optimized our system to use 12 ROIs, 3-s EEG epochs, and three letter stimuli, respectively.

TABLE IV

IDENTIFICATION ACCURACY AND COMPUTING TIME (MEAN ± S.T.D.) AS A FUNCTION OF THE NUMBER OF LETTER STIMULI WITH 12 ROIS AND A 3-S EEG EPOCH SIZE

# of stimuli	Accuracy (%)	Computing time (s)
1	65.67 ± 3.66	3.09 ± 0.10
2	80.84 ± 2.42	6.11 ± 0.15
3	86.39 ± 2.60	9.13 ± 0.21
4	89.11 ± 2.26	12.19 ± 0.25
5	92.70 ± 2.37	15.18 ± 0.37
6	95.14 ± 1.52	18.39 ± 0.42

IV. DISCUSSION

Using causal neurodynamic connectivity based on top-down cognitive EEG features, we obtained considerably higher decoding accuracy for the identification of individuals (98.60% on average in the 16-ROI, 5-s EEG epoch condition) compared to previous studies using EEG-based individual-identification approaches. This study proposes a novel method for decoding individual identity using a newly proposed SSVEP-based cognitive EEG paradigm [12]. Although the total time needed to complete this technique can still be improved, it has shown promising results, building toward future identification technology that is resistant to forgery due to the authentic and unique characteristics of individual neurodynamics.

Among all the experimental parameter combinations, we observed that the parameter set with the 5-s EEG epoch, 16 ROIs and all six stimuli led to maximal identification performance. This is because greater temporal and spatial information regarding all the stimuli would improve decoding performance. For instance, since we analyzed EEG attributes in a frequency domain (5–14 Hz) to compute brain causal brain connectivity, a reasonable time duration is a prerequisite for obtaining EEG spectral components for each frequency band. That is, a reasonable period that includes a sufficient number of intact wavelengths of these frequencies should be taken into consideration for further analyses. In addition, more ROIs allow more differentiated patterns of causal brain connectivity (i.e., DTF matrices), which consequently increases the number of discriminative features, leading to better and easier identification.

In addition to the number of letter stimuli and EEG epoch size, both contributing to the length of stimulus duration, the computation of causal brain connectivity is another substantial factor that modulates processing time for this identification system. As described in Section III-D, although results under the 3-s EEG epoch, 12-ROI parameter combination (an economically optimal condition) did not yield maximal individual identification accuracy; the accuracy rate resulting from this condition using three letter stimuli (86.39%) is relatively acceptable, as both the computing (9.13 s) and presentation times (15 s = 3 letters × 5 s for each letter) are regarded as reasonable for practical application (Table IV). When more parameters were included for identification performance, the system consequently needed more computing time, which is unsuitable for practical systems, despite further improvements in accuracy. Thus, since there is a trade-off between accuracy and computing time (see Table IV), the above parameter set was proposed as an optimal candidate for practical usage of this system.

It is noteworthy that the most active parts of selected ROIs (BA 24 and 27) in this system were subcortical top-down brain regions. BA 24 is the anterior cingulate cortex (ACC), which executes top-down inhibitory control [42], [43], conflict monitoring [44]–[46], and attention [47]. BA 27 is the hippocampal/parahippocampal region associated with short-term memory processing [48]. Because causal connectivity generated predominantly from these areas was prominently activated during the performance of this task, neurophysiological evidence supports that the present technology involves ACC/hippocampal-based top-down cognitive processing. Although La Rocca *et al.* [49] have already used EEG spectral coherence connectivity for human brain distinctiveness, the authors employed a simple eye open/closed resting condition, contrasted with the higher-order top-down processing condition in this study. Moreover, simple coherence analysis cannot provide directional causality among ROIs, whereas our study has explicitly shown directional causality from the ACC and hippocampus to other brain regions. Neurodynamic indices particularly based on such subcortical brain regions as BA 24 and 27 in the present study are also advantageous for patients whose sensorimotor cortical areas are damaged, which reduces the reliability of typical brain signals derived therein for EEG-mediated individual identification.

Other ROIs involved in this study also have significant roles in top-down processing. For instance, BA 32 is the dorsal ACC, the ventral part of which is BA 24. BA 9 is the dorsolateral prefrontal cortex (DLPFC), which is essential for higher-order cognitive control functions and promotes active manipulation and monitoring of sensorimotor information mechanisms in working memory [50]. The DLPFC is also involved in representing cognitive action and goal-directed behaviors [51], [52]. BA 29 is the granular retrolimbic area, which is near the visual areas and the hippocampal memory system. BA 40 is Wernicke's area, which is the key region for language comprehension. BA 41 closely corresponds to the primary auditory cortex. Processing of the conceived letter in the current study may evoke auditory or linguistic activation.

This identification system essentially accesses and uses intentional top-down cognitive systems, allowing for the exploration of potent EEG-based identification technology that can decode a variety of human intentions. This system can lead to an expanded repertoire of brain-fingerprint techniques and thus open new EEG-based authentication and security technologies. For example, multi-factor authentication mechanisms are required to enforce strong authentication based on biometrics and identifiers of another nature. The identification scheme of this study can serve as one of the robust and effective biometric components of multi-factor authentication. As compared with physically-driven bottom-up processing, top-down processing better reflects individuals' characteristic mental states. Accordingly, it can be efficiently used as a precise and potent brain fingerprint.

This technology can be applied to forensics and security devices in everyday life. For instance, if the SSVEP-inducing grid-shaped flickering line array is embedded in a small display on a door lock, the door will open only when it recognizes a designated master's causal EEG connectivity patterns. Alternatively, a TV remote controller can recognize its owner by analyzing a neurodynamic EEG fingerprint when the system is embedded in a display on its remote control. Further refinement by adding more rows and columns to the grid-shaped line array (which enables the decoding of a larger set of letter-like shapes) would, in principle, allow this technology to accomplish more advanced discrimination tasks consistently and reliably.

However, this system requires further improvement in subsequent studies. The constraints of this study are as follows: First, since a larger sample size would result in a higher statistical power, the present study with a sample size of 20 warrants further investigation. Thus, the present observations should be interpreted carefully while considering this statistical limitation. Second, decoding time should still be improved. Currently, our system needs 9.13 s of computing time for individual identification in the 12-ROI, 3-s EEG epoch, 3-letter stimulus condition. By using further differentiable SSVEP-inducing stimuli and parallel processing, computing time will be further decreased, resulting in a more practical EEG-based identification technology. Third, the flicker stimulation can produce visual fatigue or discomfort [53]. However, this can be overcome using high-frequency SSVEP technology [54], [55]. Flickering at high-frequencies produces much less visual fatigue than at lower frequencies [56], [57], making SSVEP-based identification more comfortable and stable [56]. Fourth, although the present study used wet EEG electrodes, dry electrodes can be employed for wearable and convenient use in practical situations. Lastly, as the grid-shaped SSVEP technique is currently implemented using the Korean letter system, a study in which it is transferred to other languages is required to ensure its versatility.

V. Conclusion

The proposed neurodynamic connectivity-based user-recognition system may become a potent future technology for individual identification. Unlike most previous studies

in SSVEP-based neurotechnology, which inevitably require macroscopic ocular movements [19], the present top-down SSVEP paradigm uses a highly compact stimulus presentation. Therefore, our novel EEG-based forensics and security paradigm provides a gaze-shift-free identification technique. This novel approach could, in principle, use top-down cognitive features analyzed by individuals' characteristic neurodynamic causal connectivity—a technique that may ultimately become useful for future forensics and security techniques. This study demonstrates that human top-down EEG signals provide promising and potent individual identification features that enable practical and versatile user-recognition applications.

ACKNOWLEDGMENT

The authors are grateful to Sejik Park and Insoo Kim for their assistance during EEG acquisition.

REFERENCES

[1] K. Cao, X. Yang, X. J. Chen, Y. L. Zang, J. M. Liang, and J. Tian, "A novel ant colony optimization algorithm for large-distorted fingerprint matching," *Pattern Recognit.*, vol. 45, pp. 151–161, Jan. 2012.

[2] H. Zhang, N. M. Nasrabadi, Y. Zhang, and T. S. Huang, "Joint dynamic sparse representation for multi-view face recognition," *Pattern Recognit.*, vol. 45, no. 4, pp. 1290–1298, Apr. 2012.

[3] A. K. Jain, A. Ross, and S. Pankanti, "Biometrics: A tool for information security," *IEEE Trans. Inf. Forensics Security*, vol. 1, no. 2, pp. 125–143, Jun. 2006.

[4] P. Campisi and D. La Rocca, "Brain waves for automatic biometric-based user recognition," *IEEE Trans. Inf. Forensics Security*, vol. 9, no. 5, pp. 782–800, May 2014.

[5] R. B. Paranjape, J. Mahovsky, L. Benedicenti, and Z. Koles, "The electroencephalogram as a biometric," in *Proc. Can. Conf. Elect. Comput. Eng.*, 2001, pp. 1363–1366.

[6] S. Marcel and J. D. R. Millan, "Person authentication using brainwaves (EEG) and maximum *a posteriori* model adaptation," *IEEE Trans. Pattern Anal. Mach. Intell.*, vol. 29, no. 4, pp. 743–748, Apr. 2007.

[7] Q. Zhao *et al.*, "Improving individual identification in security check with an EEG based biometric solution," in *Proc. Int. Conf. Brain Inf.*, 2010, pp. 145–155.

[8] M. Poulos, M. Rangoussi, V. Chrissikopoulos, and A. Evangelou, "Person identification based on parametric processing of the EEG," in *Proc. 6th IEEE Int. Conf. Elect. Circuits Syst.*, 1999, pp. 283–286.

[9] S.-K. Yeom, H.-I. Suk, and S.-W. Lee, "Person authentication from neural activity of face-specific visual self-representation," *Pattern Recognit.*, vol. 46, no. 4, pp. 1159–1169, 2013.

[10] Y. Chen *et al.*, "A high-security EEG-based login system with RSVP stimuli and dry electrodes," *IEEE Trans. Inf. Forensics Security*, vol. 11, no. 12, pp. 2635–2647, Dec. 2006.

[11] J. D. Haynes and G. Rees, "Decoding mental states from brain activity in humans," *Nature Rev. Neurosci.*, vol. 7, pp. 523–534, Jul. 2006.

[12] B. K. Min, S. Döhne, M. H. Ahn, Y. K. Noh, and K. R. Müller, "Decoding of top-down cognitive processing for SSVEP-controlled BMI," *Sci. Rep.*, vol. 6, p. 36267, Nov. 2016, doi: 10.1038/srep36267.

[13] R. Palaniappan and D. P. Mandic, "EEG based biometric framework for automatic identity verification," *J. VLSI Signal Process. Syst. Signal Image Video Technol.*, vol. 49, pp. 243–250, Nov. 2007.

[14] A. Kübler and K.-R. Müller, "An introduction to brain–computer interfacing," in *Towards Brain-Computer Interfacing*, G. Dornhege, J. D. R. Millán, T. Hinterberger, D. McFarland, and K.-R. Müller, Eds. Cambridge, MA, USA: MIT Press, 2007, pp. 1–25.

[15] J. R. Wolpaw and E. W. Wolpaw, "Brain–computer interfaces: Something new under the sun," in *Brain-Computer Interfaces: Principles and Practice*, J. R. Wolpaw and E. W. Wolpaw, Eds. New York, NY, USA: Oxford Univ. Press, 2012, pp. 3–12.

[16] B. K. Min, M. J. Marzelli, and S. S. Yoo, "Neuroimaging-based approaches in the brain-computer interface," *Trends Biotechnol.*, vol. 28, pp. 552–560, Nov. 2010.

[17] P. L. Nunez and R. Srinivasan, "Steady-state visually evoked potentials," in *Electric Fields of the Brain: The Neurophysics of EEG*, P. L. Nunez and R. Srinivasan, Eds., 2nd ed. New York, NY, USA: Oxford Univ. Press, 2006, pp. 402–409.

[18] M. Cheng, X. Gao, S. Gao, and D. Xu, "Design and implementation of a brain-computer interface with high transfer rates," *IEEE Trans. Biomed. Eng.*, vol. 49, no. 10, pp. 1181–1186, Oct. 2002.

[19] F. B. Vialatte, M. Maurice, J. Dauwels, and A. Cichocki, "Steady-state visually evoked potentials: Focus on essential paradigms and future perspectives," *Prog. Neurobiol.*, vol. 90, pp. 418–438, Apr. 2010.

[20] N.-S. Kwak, K.-R. Müller, and S.-W. Lee, "A lower limb exoskeleton control system based on steady state visual evoked potentials," *J. Neural Eng.*, vol. 12, p. 056009, 2015.

[21] L. Acqualagna *et al.*, "EEG-based classification of video quality perception using steady state visual evoked potentials (SSVEPs)," *J. Neural Eng.*, vol. 12, no. 5, p. 026012, 2015.

[22] G. R. Müller-Putz and G. Pfurtscheller, "Control of an electrical prosthesis with an SSVEP-based BCI," *IEEE Trans. Biomed. Eng.*, vol. 55, no. 1, pp. 361–364, Jan. 2008.

[23] I. Kaashoek, "Automatic determination of the optimum stimulation frequencies in an SSVEP based BCI," Koninklijke Philips Electron., Amsterdam, The Netherlands, Tech. Rep. TN-2008/00511, 2008.

[24] X. Gao, D. Xu, M. Cheng, and S. Gao, "A BCI-based environmental controller for the motion-disabled," *IEEE Trans. Neural Syst. Rehabil. Eng.*, vol. 11, no. 12, pp. 40–137, Jun. 2003.

[25] M. A. Pastor, J. Artieda, J. Arbizu, M. Valencia, and J. C. Masdeu, "Human cerebral activation during steady-state visual-evoked responses," *J. Neurosci.*, vol. 23, pp. 11621–11627, Dec. 2003.

[26] X. Chen, Z. Chen, S. Gao, and X. Gao, "A high-ITR SSVEP-based BCI speller," *Brain-Comput. Interfaces*, vol. 1, nos. 3–4, pp. 181–191, 2014.

[27] S. Makeig, T.-P. Jung, A. J. Bell, D. Ghahremani, and T. J. Sejnowski, "Blind separation of auditory event-related brain responses into independent components," *Proc. Nat. Acad. Sci. USA*, vol. 94, no. 20, pp. 10979–10984, 1997.

[28] A. A. Ioannides, "Dynamic functional connectivity," *Current Opinion Neurobiol.*, vol. 17, pp. 161–170, Apr. 2007.

[29] B. He, Y. K. Dai, L. Astolfi, F. Babiloni, H. Yuan, and L. Yang, "eConnectome: A MATLAB toolbox for mapping and imaging of brain functional connectivity," *J. Neurosci. Methods*, vol. 195, pp. 261–269, Feb. 2011.

[30] C. W. J. Granger, "Investigating causal relations by econometric models and cross-spectral methods," *Econometrica*, vol. 37, no. 3, pp. 414–417, 1969.

[31] F. Babiloni *et al.*, "Estimation of the cortical functional connectivity with the multimodal integration of high-resolution EEG and fMRI data by directed transfer function," *Neuroimage*, vol. 24, no. 1, pp. 118–131, Jan. 2005.

[32] L. Astolfi *et al.*, "Comparison of different cortical connectivity estimators for high-resolution EEG recordings," *Human Brain Mapping*, vol. 28, pp. 143–157, Feb. 2007.

[33] R. Kus, M. Kaminski, and K. J. Blinowska, "Determination of EEG activity propagation: Pair-wise versus multichannel estimate," *IEEE Trans. Biomed. Eng.*, vol. 51, no. 9, pp. 1501–1510, Sep. 2004.

[34] M. J. Kaminski and K. J. Blinowska, "A new method of the description of the information flow in the brain structures," *Biol. Cybern.*, vol. 65, no. 3, pp. 203–210, 1991.

[35] T. Schneider and A. Neumaier, "Algorithm 808: ARfit—A MATLAB package for the estimation of parameters and eigenmodes of multivariate autoregressive models," *ACM Trans. Math. Softw.*, vol. 27, pp. 58–65, Mar. 2001.

[36] Y. Dai, W. Zhang, D. L. Dickens, and B. He, "Source connectivity analysis from MEG and its application to epilepsy source localization," *Brain Topogr.*, vol. 25, no. 2, pp. 157–166, 2012.

[37] Y. Dai and B. He, "MEG-based brain functional connectivity analysis using eConnectome," in *Proc. 8th Int. Symp. Noninvasive Funct. Source Imag. Brain Heart 8th Int. Conf. Bioelectromagn. (NFSI, ICBEM)*, 2011, pp. 9–11.

[38] L. Ding, G. A. Worrell, T. D. Lagerlund, and B. He, "Ictal source analysis: Localization and imaging of causal interactions in humans," *Neuroimage*, vol. 34, pp. 575–586, Jan. 2007.

[39] D. Garrett, D. A. Peterson, C. W. Anderson, and M. H. Thaut, "Comparison of linear, nonlinear, and feature selection methods for EEG signal classification," *IEEE Trans. Neural Syst. Rehabil. Eng.*, vol. 11, no. 2, pp. 141–144, Jun. 2003.

[40] C. Guerrero-Mosquera, M. Verleysen, and A. Navia-Vazquez, "Dimensionality reduction for EEG classification using mutual information and SVM," in *Proc. IEEE Int. Workshop Mach. Learn. Signal Process.*, Beijing, China, Sep. 2011, pp. 1–6.

[41] Y. Benjamini and Y. Hochberg, "Controlling the false discovery rate: A practical and powerful approach to multiple testing," *J. Roy. Statist. Soc., Ser. B*, vol. 57, pp. 289–300, Jan. 1995.
[42] R. L. Silton *et al.*, "The time course of activity in dorsolateral prefrontal cortex and anterior cingulate cortex during top-down attentional control," *Neuroimage*, vol. 50, pp. 1292–1302, Apr. 2010.
[43] K. Johnston, H. M. Levin, M. J. Koval, and S. Everling, "Top-down control-signal dynamics in anterior cingulate and prefrontal cortex neurons following task switching," *Neuron*, vol. 53, pp. 453–462, Feb. 2007.
[44] V. M. Borsa *et al.*, "Interference and conflict monitoring in individuals with amnestic mild cognitive impairment: A structural study of the anterior cingulate cortex," *J. Neuropsychol.*, May 2016. [Online]. Available: http://onlinelibrary.wiley.com/doi/10.1111/jnp.12105/full
[45] M. M. Botvinick, J. D. Cohen, and C. S. Carter, "Conflict monitoring and anterior cingulate cortex: An update," *Trends Cognit. Sci.*, vol. 8, no. 12, pp. 539–546, 2004.
[46] M. A. Apps, J. H. Balsters, and N. Ramnani, "The anterior cingulate cortex: Monitoring the outcomes of others' decisions," *Soc. Neurosci.*, vol. 7, pp. 424–435, Jul. 2012.
[47] R. Lane, E. Reiman, B. Axelrod, L. Yun, A. Holmes, and G. Schwartz, "Neural correlates of levels of emotional awareness: Evidence of an interaction between emotion and attention in the anterior cingulate cortex," *J. Cognit. Neurosci.*, vol. 10, no. 4, pp. 525–535, Jul. 1998.
[48] R. P. Vertes, "Hippocampal theta rhythm: A tag for short-term memory," *Hippocampus*, vol. 15, no. 7, pp. 923–935, 2005.
[49] D. La Rocca *et al.*, "Human brain distinctiveness based on EEG spectral coherence connectivity," *IEEE Trans. Biomed. Eng.*, vol. 61, no. 9, pp. 2406–2412, Sep. 2014.
[50] B. L. Miller and J. L. Cummings, *The Human Frontal Lobes: Functions and Disorders*, 2nd ed. New York, NY, USA: Guilford Press, 2007.
[51] D. McNamee, M. Liljeholm, O. Zika, and J. P. O'Doherty, "Characterizing the associative content of brain structures involved in habitual and goal-directed actions in humans: A multivariate fMRI study," *J. Neurosci.*, vol. 35, no. 9, pp. 3764–3771, 2015.
[52] J. M. Fuster, *The Prefrontal Cortex: Anatomy, Physiology, and Neuropsychology of the Frontal Lobe*, 2nd ed. New York, NY, USA: Raven, 1989.
[53] D. Zhu, J. Bieger, G. Garcia Molina, and R. M. Aarts, "A survey of stimulation methods used in SSVEP-based BCIs," *Comput. Intell. Neurosci.*, vol. 2010. pp. 7023–7057, Jan. 2010.
[54] P. F. Diez *et al.*, "Commanding a robotic wheelchair with a high-frequency steady-state visual evoked potential based brain–computer interface," *Med. Eng. Phys.*, vol. 35, no. 8, pp. 1155–1164, 2013.
[55] P. F. Diez, V. A. Mut, E. M. A. Perona, and E. L. Leber, "Asynchronous BCI control using high-frequency SSVEP," *J. Neuroeng. Rehabil.*, vol. 8, p. 39, Jul. 2011.
[56] W. Yijun, W. Ruiping, G. Xiaorong, and G. Shangkai, "Brain-computer interface based on the high-frequency steady-state visual evoked potential," in *Proc. 1st Int. Conf. Neural Interface Control*, Wuhan, China, 2005, pp. 37–39.
[57] A. Materka, M. Byczuk, and P. Poryzala, "A virtual keypad based on alternate half-field stimulated visual evoked potentials," in *Proc. Int. Symp. Inf. Technol. Converg. (ISITC)*, Jeon Ju, Korea, 2007, pp. 296–300.

Byoung-Kyong Min (M'12) received the M.S. degree in neurobiology and physiology from Northwestern University, Evanston, IL, USA, in 1998, and the Ph.D. degree in biological psychology from Magdeburg University, Germany, in 2007. From 2007 to 2009, he was a Post-Doctoral Fellow with the Yonsei University College of Medicine (Severance Hospital), Seoul, South Korea. From 2009 to 2011, he was a Research Fellow with the Harvard Medical School (Brigham & Women's Hospital), Boston, MA, USA. Since 2012, he has been an Assistant Professor with the Department of Brain and Cognitive Engineering, Korea University, Seoul. His research interests include spectral analysis of brain electrical activity (EEG) and EEG-based brain–machine interfaces (BMIs). He has combined ultrasound sonication with an EEG-based BMI to accomplish a non-invasive human brain-to-brain interface. He serves as an Editor of the journal *Medicine* and a Publication Chair of two IEEE international conferences and workshops.

Heung-Il Suk (S'08–M'12) received the B.S. and M.S. degrees in computer engineering from Pukyong National University, Busan, South Korea, in 2004 and 2007, respectively, and the Ph.D. degree in computer science and engineering from Korea University, Seoul, South Korea, in 2012. From 2012 to 2014, he was a Post-Doctoral Research Associate with the University of North Carolina at Chapel Hill, USA. Since 2015, he has been a Tenure-Track Assistant Professor with the Department of Brain and Cognitive Engineering, Korea University. His research interests include machine learning, computer-aided brain disease diagnosis, medical image analysis, and brain–computer interfaces.

Min-Hee Ahn (S'16) received the master's degree in computer engineering from Pusan National University, South Korea, in 1998, and the Ph.D. degree in neuroscience from the University of Seoul Buddha in 2010, with a thesis on brainwave-based brain healthcare system R&D. He is currently pursuing the Ph.D. degree with the Department of Brain and Cognitive Engineering, Korea University, with a focus on brain–machine interfaces and neurofeedback systems. From 2004 to 2014, he developed EEG and neurofeedback solutions at the company, Panaxtos, as the CTO and accumulated practical brainwave research experience with embedded hardware and software. He has a national license in professional engineering, and has contributed to a Korean bio-health standard roadmap on smart healthcare organized by the Korean Government.

Min-Ho Lee received the B.S. degree in computer science and engineering from Seokyeong University, Seoul, South Korea, in 2012. He is currently pursuing the Ph.D. degree with the Department of Brain and Cognitive Engineering, Korea University, Seoul. His current research interests include machine learning, brain–computer interfaces, and neurofeedback systems. He received the Bronze Award at the 22th Samsung Human-Tech Thesis Prize in 2016.

Seong-Whan Lee (S'84–M'89–SM'96–F'10) received the B.S. degree in computer science and statistics from Seoul National University, South Korea, in 1984, and the M.S. and Ph.D. degrees in computer science from the Korea Advanced Institute of Science and Technology, Seoul, South Korea, in 1986 and 1989, respectively. He is currently the Hyundai-Kia Motor Chair Professor with Korea University, Seoul, where he is also the Head of the Department of Brain and Cognitive Engineering. His research interests include artificial intelligence, pattern recognition, and brain engineering. He is a fellow of the IAPR and the Korean Academy of Science and Technology.